Molecular structure and vibrational spectroscopic investigation of melamine using DFT theory calculations

ARTICLE *in* SPECTROCHIMICA ACTA PART A MOLECULAR AND BIOMOLECULAR SPECTROSCOPY · DECEMBER 2013

Impact Factor: 2.35 · DOI: 10.1016/j.saa.2013.12.056 · Source: PubMed

4 AUTHORS, INCLUDING:

Sethu Gunasekaran
St. Peter's University
220 PUBLICATIONS **1,265** CITATIONS
SEE PROFILE

Srinivasan S
Presidency College
33 PUBLICATIONS **128** CITATIONS
SEE PROFILE

Spectrochimica Acta Part A: Molecular and Biomolecular Spectroscopy 123 (2014) 392–401

Contents lists available at ScienceDirect

Spectrochimica Acta Part A: Molecular and Biomolecular Spectroscopy

journal homepage: www.elsevier.com/locate/saa

Molecular structure and vibrational spectroscopic investigation of melamine using DFT theory calculations

M. Prabhaharan [a,b], A.R. Prabakaran [b], S. Gunasekaran [c], S. Srinivasan [d,*]

[a] Department of Physics, Aksheyaa College of Engineering, Puludivakkam, India
[b] PG and Research Department of Physics, Pachaiyappa's College, Chennai, India
[c] R & D Center, St. Peter's University, Chennai, India
[d] PG and Research Department of Physics, Presidency College, Chennai, India

HIGHLIGHTS

- Spectroscopic properties of melamine were examined by FT-IR, FT-Raman techniques and DFT methods.
- NBO analysis used to explain the interaction between electron donors and acceptors.
- HOMO and LUMO energies, MEP distribution of the molecule were calculated.
- The atomic charges on the various atoms of molecule were obtained by Mulliken population analysis.

GRAPHICAL ABSTRACT

Melamine crystals block the small tubes in the kidney potentially stopping the production of urine, causing kidney failure. The equilibrium geometry harmonic vibrational frequencies, IR intensities and Raman scattering activities were calculated by density functional (B3LYP) method with 6-31G(d,p) and 6-311++G(d,p) basis sets, using Gaussian 03W program. HOMO and LUMO energies are calculated that these energies confirm charge transfer occurs within the molecule.

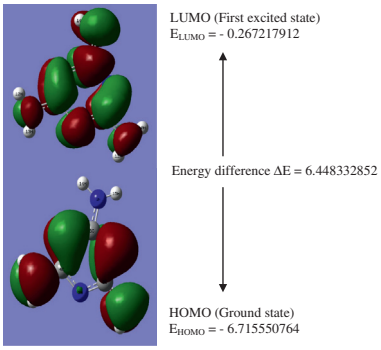

ARTICLE INFO

Article history:
Received 20 October 2013
Received in revised form 18 November 2013
Accepted 5 December 2013
Available online 18 December 2013

Keywords:
Melamine
FT-Raman
FT-IR
DFT
HOMO–LUMO
NBO

ABSTRACT

The FT-Raman and FT-IR spectra for melamine have been recorded in the region 4000–100 cm^{-1} and 4000–400 cm^{-1}, respectively compared with the harmonic vibrational frequencies calculated using density functional theory method (B3LYP) by employing 6-31G(d,p) and 6-311++G(d,p) basis set with appropriate scaling factors. Optimized geometries of the molecule have been interpreted and compared with the reported experimental values. The experimental geometrical parameters prove satisfactory concurrence with the theoretical prediction from DFT. The scaled vibrational frequencies seem to coincide with the experimentally observed values with acceptable deviations. The theoretical spectrograms have been constructed and compared with the experimental FT-Raman and FT-IR spectra. The calculated Highest Occupied Molecular Orbital (HOMO) and Lowest Unoccupied Molecular Orbital (LUMO) energies show that charge transfer occurs in the molecule. The first order hyperpolarizability β_{total} of this molecular system and related properties (α, β, μ and $\Delta\alpha$) are calculated using DFT/B3LYP/6-31G(d,p) and 6-311++G(d,p) basis set based on the finite-field approach. Stability of the molecule arising from hyper conjugative interaction, charge delocalization has been analyzed using natural bond orbital (NBO) analysis. Thermodynamic properties like entropy, heat capacity and zero-point energy have been calculated for the molecule.

* Corresponding author. Tel.: +91 9884766203.
E-mail address: dr_s_srinivasan@yahoo.com (S. Srinivasan).

1386-1425/$ - see front matter © 2013 Elsevier B.V. All rights reserved.
http://dx.doi.org/10.1016/j.saa.2013.12.056

Introduction

Melamine is an organic chemical ($C_3H_6N_6$) commonly found in the form of white crystals rich in nitrogen. Melamine is widely used in plastics, adhesives, countertops, dishware, and white-boards. Melamine resin is often used in kitchen utensils and plates [1–3]. When it is combined with cyanuric acid, it can form crystals that can give rise to kidney stones. These small crystals can also block the small tubes in the kidney potentially stopping the production of urine, causing kidney failure [4]. This compound became headline news recently after the occurrence of an outbreak of urinary stones in infants and children consuming melamine-tainted milk in china.

Spectroscopy and Surface Enhanced Raman Spectroscopy (SERS) investigations on melamine were reported by earlier researcher's [5,6]. But the complete analysis of vibrational band assignment using quantum chemical methods have not been reported so far. In the present study, FT-IR and FT-Raman spectral investigation of melamine molecule have been performed using density functional theory (DFT) and vibrational spectral analysis based on the calculated total energy distribution (TED). These methods predict relatively accurate molecular structure and vibrational spectra with moderate computational effort. The assignments are aided by DFT/B3LYP method using 6-31G(d,p) and 6-311++G(d,p) basis sets. The redistribution of electron density (ED) in various bonding and anti-bonding orbital and $E^{(2)}$ energies have been calculated by natural bond orbital (NBO) analysis using DFT method to give clear evidence of stabilization originating from the hyper conjugation of various intra molecular interactions.

Experimental methods

The spectroscopic pure sample of melamine was procured from reputed pharmaceutical firms in Chennai, India and used as such. The Fourier transform infrared spectrum of melamine was recorded with an ABB Bomem Series spectrometer over the region 4000–400 cm^{-1} by adopting the KBr pellet technique at Sophisticated Analytical Instrument Facility, Indian Institute of Technology Madras, Chennai, India. The FT-Raman spectrum was also recorded at Sophisticated Analytical Instrument Facility, Indian Institute of Technology Madras, Chennai, India using a BRUKER: RFS 27 spectrometer. A laser frequency of 15,798 cm^{-1} was used as an excitation source. The spectrometer is fitted with an XT-KBr beam splitter and a DTGS detector. A baseline correction was made for the spectrum recorded.

Computation details

The computations were performed at 6-31G(d,p) and 6-311++G(d,p) levels on a Pentium intel core i5 personal computer using the GAUSSIAN 03W package [7], with employing density functional methods. The optimized geometry was used in the vibrational frequency calculation at DFT level to characterize all stationary points as minima. The vibrational frequency assignments were made with a high degree of accuracy with the help of Chemcraft software program [8]. All the calculations were done for the optimized structures in gas phase. GAUSSVIEW program [9] has been considered to get visual animation and also for the verification of the normal modes assignment. The natural bonding orbitals (NBO) calculations [10,11] were performed using GAUSSIAN 03W package at the DFT/B3LYP/6-311++G(d,p) level in order to understand various second order interactions between the filled orbital of one subsystem and vacant orbitals of another subsystem, which is a measure inter molecular delocalization or hyper conjugation.

Results and discussion

Molecular geometry

Melamine was subjected to geometry optimization in the ground state. The optimized structural parameters bond length and bond angle was calculated by employing DFT method B3LYP with the basis sets 6-31G(d,p) and 6-311++G(d,p) were listed in Tables 1 and 2. The molecular structure of melamine (Fig. 1a) and optimized structure of melamine obtained from B3LYP with basis sets 6-31G(d,p) and 6-311++G(d,p) were shown in Fig. 1b and Fig. 1c respectively. From the calculated values, we can find that most of the optimized bond length and bond angles are slightly smaller than the experimental values [12], due to this the theoretical calculation belongs to the isolated molecules in the gaseous phase whereas the experimental results belongs to the molecules in the solid phase. It is observed that there is an appreciable bond angle difference and insignificant bond length difference is observed in both the basis set.

Table 1
Selected bond length values of melamine.

Bond length (Å)	B3LYP		Expt. values[a]
	6-31G(d,p)	6-311++G(d,p)	
N_1–C_2	1.344	1.341	1.354
N_1–C_6	1.343	1.340	1.342
C_2–N_3	1.344	1.341	1.348
C_2–N_7	1.361	1.359	1.338
N_3–C_4	1.344	1.341	1.346
C_4–N_5	1.344	1.341	1.350
C_4–N_8	1.361	1.359	1.342
N_5–C_6	1.343	1.340	1.338
C_6–N_9	1.362	1.360	1.362
N_7–H_{10}	1.007	1.006	1.017
N_7–H_{11}	1.007	1.006	1.013
N_8–H_{12}	1.007	1.006	1.003
N_8–H_{13}	1.007	1.006	1.022
N_9–H_{14}	1.007	1.006	1.022
N_9–H_{15}	1.007	1.006	1.013

[a] Taken from Ref. [12].

Table 2
Selected bond angle values of melamine.

Bond angle (°)	B3LYP		Expt. values[a]
	6-31G(d,p)	6-311++G(d,p)	
C_2–N_1–C_6	113.4	113.9	114.8
N_1–C_2–N_3	126.5	126.1	124.7
N_1–C_2–N_7	116.7	116.9	117.0
N_1–C_6–N_5	126.6	126.1	125.8
N_1–C_6–N_9	116.7	116.9	116.3
N_3–C_2–N_7	116.7	116.9	118.3
C_2–N_3–C_4	113.4	113.9	114.9
C_2–N_7–H_{10}	117.5	118.2	118.4
C_2–N_7–H_{11}	117.5	118.2	118.9
N_3–C_4–N_5	126.6	126.1	125.3
N_3–C_4–N_8	116.7	117.0	117.8
N_5–C_4–N_8	116.7	116.9	116.9
C_4–N_5–C_6	113.4	113.9	114.5
C_4–N_8–H_{12}	117.4	118.3	118.5
C_4–N_8–H_{13}	117.4	118.3	119.6
N_5–C_6–N_9	116.7	116.9	117.9
C_6–N_9–H_{14}	117.3	118.0	114.4
C_6–N_9–H_{15}	117.3	118.0	115.3
H_{10}–N_7–H_{11}	119.3	119.7	119.6
H_{12}–N_8–H_{13}	119.2	119.8	119.0
H_{14}–N_9–H_{15}	119.1	119.5	113.9

[a] Taken from Ref. [12].

(a) *Molecular structure of melamine*

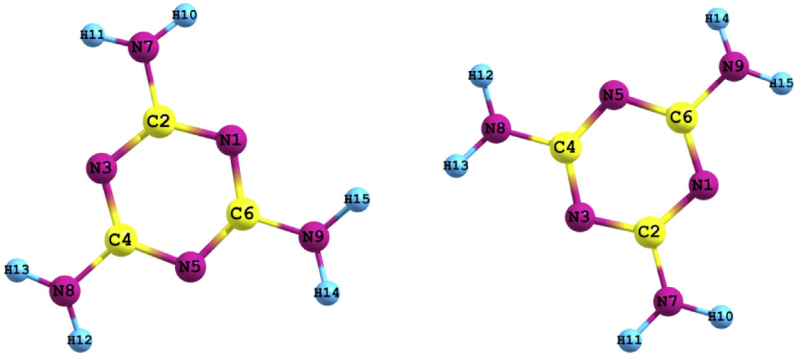

(b) (c)

Fig. 1. (a) Molecular structure and atom numbering scheme of melamine, (b) 6-31G(d,p), and (c) 6-311++G(d,p) basis sets.

Conformational analysis

The accurate determination of geometrical distortions is an important tool for investigating the nature of intra and intermolecular interactions. Conformational analysis was performed in order to define the preferential position of melamine with respect to the NH_2 rotation of the title molecule. The possible conformers of melamine depend on the rotation of amine group linked to the ring. The potential energy barrier obtained by the rotation of the amine group with dihedral angle N_1–C_2–N_7–H_{10} of melamine using B3LYP/6-31G(d,p) method is given in Fig. 2. These bonds are responsible for the flexibility and conformational stability of melamine. Thus a search of low energy structure are performed, it is relevant coordinate for conformational flexibility within the molecule. During the calculation all the geometrical parameters were simultaneously relaxed while the N_1–C_2–N_7–H_{10} torsional angles were varied steps of 15° up to 360°. The compound has three different conformations. The stability of the conformers is in the order I > III > II. For this rotation minimum energy curve has been obtained at 14° with the minimum energy of −446.51198 A.U. The energy difference between the most stable (I) and the second stable (III) conformations is 0.00196 A.U. The conformer II is the unstable transition structure. Therefore, in the present work we have focussed on the most stable form of melamine molecule to clarify molecular assignments of vibrational spectra.

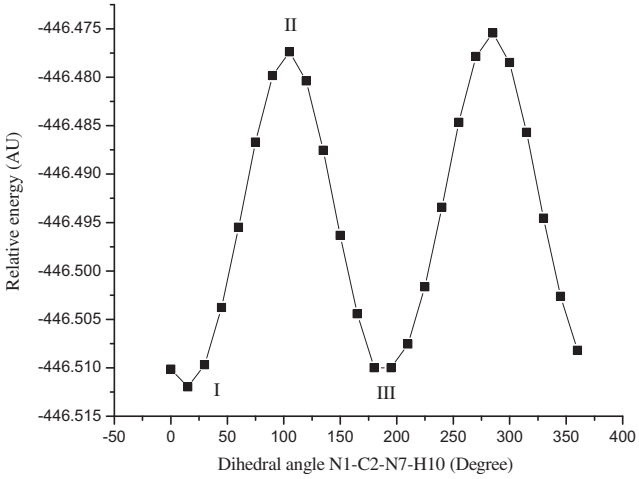

Fig. 2. PES scan for dihedral angle N_1–C_2–N_7–H_{10} of melamine at B3LYP/6-31G(d,p).

Vibrational spectra

According to the theoretical calculations, the title compound belongs to C1 point group symmetry. Melamine consists of 15 atoms and hence 39 normal modes of vibrations were possible according to the 3N-6 rule. All these modes of vibrations were active in both IR and Raman spectra. All the vibrational assignments of fundamental modes of melamine along with the calculated IR and Raman frequencies and normal mode description are presented in Table 3. The small difference between the experimental and calculated vibrational modes is observed. This discrepancy can come from the formation of intermolecular hydrogen bonding.

Also we note that the experimental result belongs to the solid phase and the theoretical calculation belongs to the gaseous phase. The FT-IR and FT-Raman spectra of melamine are shown in Figs. 3 and 4 respectively.

C–N Vibrations – To identify the C–N stretching frequency is a rather difficult task from other vibrations. Silverstein et al. [13] assigned C–N stretching absorption in the region 1382–1266 cm^{-1}. In benzortrizole, the C–N stretching bands are found to be present at 1307 and 1382 cm^{-1}. Shanmugam and Sathyanarayana [14] have reported the C–N stretching frequency observed at 1368 cm^{-1}. The same stretching vibration has been predicted at 1335 cm^{-1} in 2,4-dinitrophenyl hydrogen [15]. Mani et al. [16] assigned C–N stretching absorption at 1169 cm^{-1} in FT-IR and 1120 cm^{-1} in FT-Raman. The C–N stretching usually lies in the region 1400–1200 cm^{-1}. In this present study, the C–N stretching vibrations of melamine are identified between 1652–1440 cm^{-1} in IR and 1556–1443 cm^{-1} in the FT-Raman spectrum. These assignments made in this study are also supported by the literature [17]. The band observed at 582 cm^{-1} in Raman and 585 cm^{-1} in IR is assigned for C–N–C trigonal bending and Raman band with medium intensity found at 378 cm^{-1} is assigned for C–N–C ring breathing mode in H–N–C–N torsional mode of vibration. These assignments are in line with literature [18].

N–H Vibrations – In all the heterocyclic compounds, the N–H stretching vibrations occur in the region 3500–3300 cm^{-1}. Theoretically, intensity of N–H band is found to be weaker than that of O–H which is in good agreement with the experimental results. Hence in the present investigation, the N–H stretching vibration of melamine is identified at 3375 cm^{-1} in the DFT results.

Frontier molecular orbital analysis

Molecular orbitals (HOMO–LUMO) and their properties such as energy are very useful for physicists and chemists and are very important parameters for quantum chemistry. This is also used by the frontier electron density for predicting the most reactive position in π-electron systems and also explains several types of reaction in conjugated system [19]. The conjugated molecules are characterized by a small highest occupied molecular orbital-lowest unoccupied molecular orbital (HOMO–LUMO) separation, which is the result of a significant degree of intramolecular charge transfer from the end-capping electron-donor groups to the efficient electron-acceptor groups through π-conjugated path [20]. Both the highest occupied molecular orbital and lowest unoccupied molecular orbital are the main orbitals which take part in chemical stability. The HOMO represents the ability to donate an electron, LUMO as an electron acceptor, represents the ability to obtain an electron. The HOMO and LUMO energy calculated by B3LYP/6-31G(d,p) and B3LYP/6-311++G(d,p) method is shown in Table 4. This electronic absorption corresponds to the transition from the

Table 3
Observed and calculated IR wavenumbers of melamine.

Observed wavenumbers (cm^{-1})		Calculated wavenumbers (cm^{-1})						Vibrational assignments (PEDs)
		B3LYP/6-31G(d,p)			B3LYP/6-311++G(d,p)			
FTIR	FT-Raman	Unscaled	Scaled	Intensity	Unscaled	Scaled	Intensity	
		185	167	0	134	121	13	τ NH2 (17)
		186	167	0	178	161	3	τ NH2 (16)
		208	187	3	183	164	2	τ NH2 (16)
		300	270	15	197	177	28	τ HNCN (36)
		326	294	49	205	184	2	τ HNCN (39)
	233	336	303	1	238	214	29	τ HNCN (25)
		336	303	6	337	303	1	τ HNCN (23)
	378	343	309	15	337	304	1	τ HNCN (24)
		502	452	0	516	464	0	τ HNCN (21)
529		532	479	1	537	483	1	τ CNCN (14)
541		534	481	1	542	488	0	τ NCNC (20)
		562	505	0	555	499	0	τ CNCN (15)
		585	526	1	585	526	0	β CNC *op* (63)
585	582	585	526	1	585	526	0	β CNC *op* (64)
615	675	683	614	0	681	613	0	β CNC *ip* (71)
734		740	666	0	745	671	0	β CNC *ip* (56)
762	778	741	666	0	746	671	0	β NCN *op* (60)
871		828	745	7	829	746	4	β CNC *ip* (67)
	983	991	892	0	989	891	0	β HNH (83)
		1008	907	2	997	897	2	β HNC *op* (62)
		1009	908	2	999	899	2	β HNH *op* (82)
1029		1159	1043	0	1146	1032	0	β HNC *ip* (61)
		1179	1061	0	1170	1053	0	β HNH *ip* (69)
		1180	1062	0	1171	1054	0	β HNC *ip* (55)
1196		1333	1200	0	1312	1180	0	β NCN *ip* (73)
1440		1481	1333	19	1465	1319	27	υ CN (64)
1466	1443	1481	1333	19	1466	1319	27	υ CN (60)
1554	1556	1519	1367	0	1506	1355	0	υ CN (64)
		1616	1454	6	1602	1442	31	υ CN (53)
		1616	1454	7	1602	1442	29	υ CN (46)
		1641	1476	100	1624	1462	100	υ CN (65)
		1641	1476	100	1625	1462	97	υ CN (53)
1652		1680	1512	0	1662	1496	0	υ CN (54)
		3619	3257	8	3614	3252	10	υ NH (93)
		3620	3258	8	3615	3254	11	υ NH (94)
		3622	3260	1	3617	3255	2	υ NH (90)
		3758	3382	4	3746	3371	5	υ NH (91)
		3760	3384	4	3748	3374	6	υ NH (85)
3882		3761	3385	5	3750	3375	6	υ NH (86)

Note: υ – stretching; β – bending (*ip* – in plane, *op* – out of plane); τ – torsion.

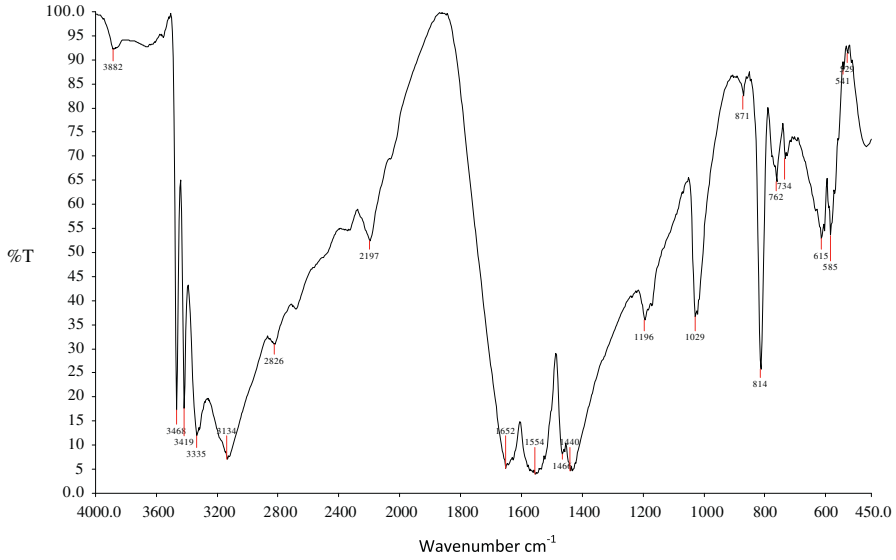

Fig. 3. Experimental FTIR spectrum of melamine.

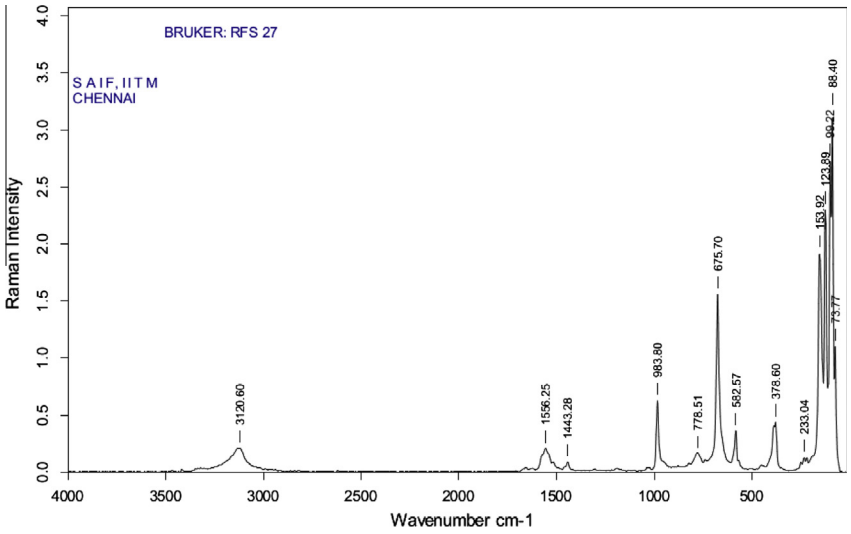

Fig. 4. Experimental FT-Raman spectrum of melamine.

ground to the first excited state and is mainly described by one electron excitation from the highest occupied molecular orbital to the lowest unoccupied molecular orbital. While the energy of the HOMO is directly related to the ionization potential, LUMO energy is directly related to the electron affinity. Energy difference between HOMO and LUMO orbital is called as energy gap which is an important stability for structures [21]. Recently, the energy gap between HOMO and LUMO has been used to prove the bioactivity from intramolecular charge transfer [22,23]. The plots of HOMO and LUMO are shown in Fig. 5.

Table 4
HOMO, LUMO and energy gap of melamine.

Parameters	B3LYP	
	6-31G(d,p)	6-311++G(d,p)
HOMO (eV)	−6.229823704	−6.715550764
LUMO (eV)	0.632941816	−0.267217912
ENERGY GAP (eV)	6.86276552	6.448332852

Hyperpolarizability analysis

NLO is at the future of current research because it provides the key functions of frequency shifting, optical modulation, optical switching, optical logic, and optical memory for the emerging technologies in areas such as telecommunications, signal processing, and optical interconnections [24,25]. In discussing NLO properties, the polarization of the molecule by an external radiation field is often approximated as the creation of an induced dipole moment by an external electric field. The first hyperpolarizability (β) of this novel molecular system of melamine are calculated using B3LYP/6-31G(d,p) and 6-311++G(d,p) basis sets, based on the finite field approach. In the presence of an applied electric field, the energy of a system is a function of the electric field, First hyperpolarizability is a third rank tensor that can be described by a $3 \times 3 \times 3$ matrix. The 27 components of the 3D matrix can be reduced to 10 components due to the Kleinman symmetry [26]. It can be given in the lower tetrahedral format. It is obvious that the lower part of the $3 \times 3 \times 3$ matrices is a tetrahedral. The complete equations for calculating the magnitude of total static dipole moment (μ), the

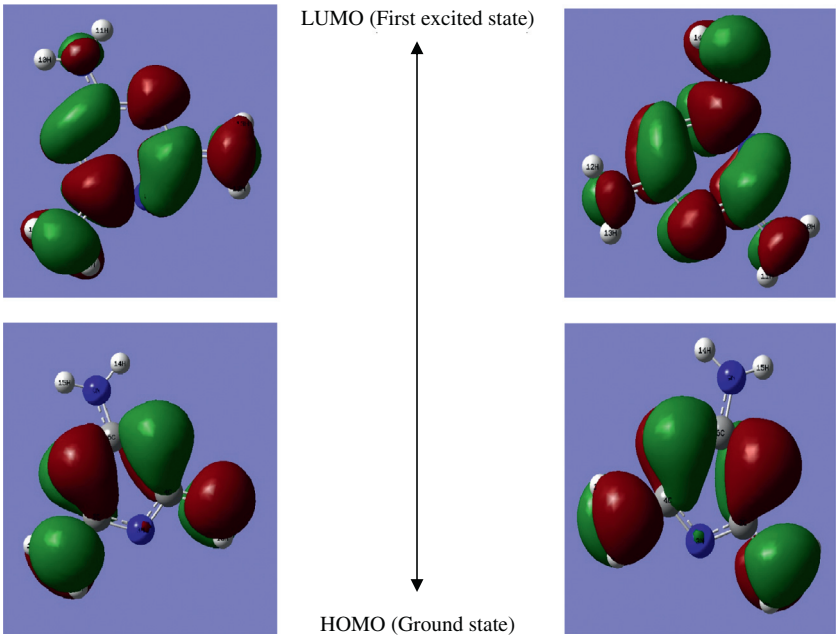

Fig. 5. The plots of HOMO and LUMO of melamine (a) DFT/B3LYP/6-31G(d,p) and (b) 6-311++G(d,p) basis sets.

mean polarizability (α), the anisotropy of the polarizability ($\Delta\alpha$) and the mean first polarizability (β), using the x, y, z components from Gaussian 03W output are as follows

$$\mu_{total} = \left(\mu_x^2 + \mu_y^2 + \mu_z^2\right)^{1/2}$$

$$\alpha = 1/3(\alpha_{xx} + \alpha_{yy} + \alpha_{zz})$$

$$\Delta\alpha = 2^{-1/2}\left[(\alpha_{xx} - \alpha_{yy})^2 + (\alpha_{yy} - \alpha_{zz})^2 + (\alpha_{zz} - \alpha_{xx})^2 6\alpha_{xx}^2\right]^{1/2}$$

$$\beta = \left(\beta_x^2 + \beta_y^2 + \beta_z^2\right)^{1/2}$$

and

$$\beta_x = \beta_{xxx} + \beta_{xyy} + \beta_{xzz}$$

$$\beta_y = \beta_{yyy} + \beta_{xxy} + \beta_{yzz}$$

$$\beta_z = \beta_{zzz} + \beta_{xxz} + \beta_{yyz}$$

The calculated hyperpolarizability values of melamine are given in Table 5. Urea is one of the prototypical molecules used in the study of NLO properties of molecular systems and frequently used as a threshold value for comparative purpose. The computed first hyperpolarizability, β_{total} of melamine molecule are 0.11060×10^{-31} cm^5/esu and 4.8221×10^{-31} cm^5/esu in B3LYP/6-31G(d,p) and 6-31++G(d,p) basis sets respectively. The second harmonic generation behavior of the melamine was tested using the Kurtz and Perry powder method. The results showed that melamine does not possess any NLO properties. Hence the B3LYP/6-31G(d,p) method polarizability results agree with experimental results, where as B3LYP/6-311++G(d,p) method overestimates the value of first order hyperpolarizability was observed. Thus, this molecule might not serve as prospective building block of NLO materials.

Mulliken population analysis

The total atomic charges of melamine obtained by Mulliken population analysis with B3LYP in different basis sets are listed in Table 6. From the result, it is clear that the substitution of NH_2

Table 5
The ab initio B3LYP/6-31G (d,p) and 6-311++G(d,p) calculated α, β and μ of melamine.

Parameters	B3LYP		Parameters	B3LYP	
	6-31G(d,p)	6-311++G(d,p)		6-31G(d,p)	6-311++G(d,p)
α_{xx}	92.6541	110.6010	β_{xxx}	106.2410	263.8790
α_{xy}	1.0779	1.2063	β_{xxy}	−10.4101	−16.4861
α_{yy}	85.9046	102.7650	β_{xyy}	−251.5950	−308.3650
α_{xz}	−2.9941	0.2923	β_{yyy}	79.6232	17.0954
α_{yz}	−0.2775	0.0387	β_{zxx}	−30.3939	37.6930
α_{zz}	34.5951	52.8754	β_{xyz}	5.6141	−3.9378
α (a.u)	71.0513	88.7471	β_{zyy}	23.8726	−40.1674
$\Delta\alpha$ (a.u)	1.6964	199.0956	β_{xzz}	37.4627	−7.7113
μ_x	−0.3398	−0.3837	β_{yzz}	−0.5334	−17.1093
μ_y	1.5644	1.7081	β_{zzz}	0.9107	−8.4177
μ_z	0.0864	0.1272	β_{tot} (a.u)	128.0192	55.8162
$\mu_{(tot)}$	1.6032	1.7553	β_{tot} (e.s.u)	0.11060×10^{-31}	4.8221×10^{-31}

Table 6
Mulliken's atomic charges of melamine performed at B3LYP method.

Atoms	Atomic charges	
	6-31G(d,p)	6-311++G(d,p)
N_1	−0.549079	−0.448546
C_2	0.639584	0.310849
N_3	−0.549462	−0.447731
C_4	0.638985	0.311726
N_5	−0.548952	−0.448615
C_6	0.637714	0.302183
N_7	−0.637181	−0.475665
N_8	−0.637010	−0.476393
N_9	−0.636834	−0.460094
H_{10}	0.273871	0.305714
H_{11}	0.273696	0.307866
H_{12}	0.273732	0.305913
H_{13}	0.273590	0.308129
H_{14}	0.273677	0.302340
H_{15}	0.273672	0.302324

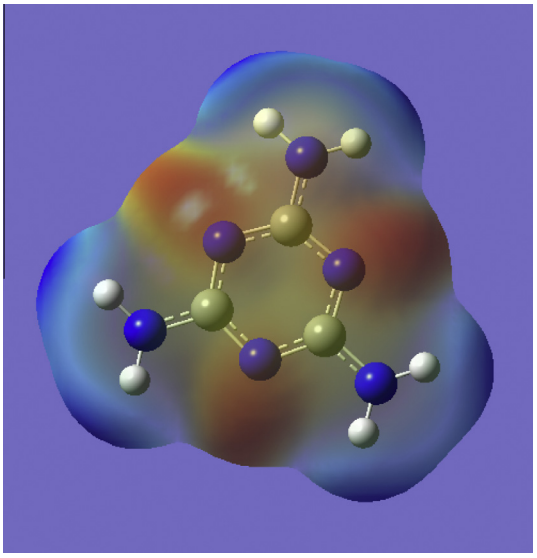

Fig. 6. The total electron density surface mapped with ESP of melamine determined by B3LYP/6-311++G(d,p) basis set.

atoms in the aromatic ring leads to a redistribution of electron density. The σ-electron withdrawing character of the nitrogen atom in melamine results the electron deficiency at C_2, C_4 and C_6 atom. The atomic charges of nitrogen atom in the NH_2 group are almost identical. The Mulliken charge obtained from 6-31G(d,p) and 6-311++G(d,p) basis set shows that C_2, C_4 and C_6 atoms are more acidic due to more positive charge.

Molecular electrostatic potential

In order to grasp the molecular interactions, the molecular electrostatic potentials (MEPs) are used. Recently, the MEPs have been used for interpreting and predicting relative reactivities sites for eletrophilic and nucleophilic attack, investigation of biological recognition, hydrogen bonding interactions, studies of zeolite, molecular cluster, crystal behavior, correlation and prediction of a wide range of macroscopic properties [27,28]. Since MEP is related to total charge distribution of the molecule and it provides the correlations between the molecular properties such as partial charges, dipole moments, electro negativity and chemical reactivity of molecules.

In this study, the electrostatic potentials at the surface represented by different colours. Red color parts represents the regions of negative electrostatic potential while blue ones represent regions of positive electrostatic potential. Additionally, green color parts represent also regions of zero potential. The negative regions of $V(r)$ potential are related to electrophiclic reactivity, while the positive ones are related to nucleophilic reactivity. MEP of melamine molecules was calculated from optimized molecular structure by using 6-311++G(d,p) level. The electrostatic potential (ESP), total electron density (ED) and molecular electrostatic potential (MEP) of the title compound is illustrated in Fig. 6.

NBO analysis

The second order Fock matrix was carried out to evaluate the donor–acceptor interactions in the NBO analysis. The interaction result is a loss of occupancy from the localized NBO of the idealized Lewis structure into an empty non-Lewis orbital. For each donor (i), and acceptor (j), the stabilization energy $E^{(2)}$ associated with the delocalization $i \rightarrow j$ is estimated as

Table 7
Second order perturbation theory analysis of Fock matrix in NBO basis of melamine.

Donor (i)	Type	ED/e (a.u)[a]	Acceptor (j)	Type	ED/e (a.u)[a]	$E^{(2)}$ (kJ mol^{-1})[b]	$E(j)-E(i)$ (a.u)[c]	$F(i,j)$ (a.u)[d]
N_1–C_2	σ	1.97860	N_1–C_6	σ*	0.03917	2.24	1.68	0.055
	σ		C_2–N_3	σ*	0.02963	2.60	1.71	0.060
	σ		C_2–N_7	σ*	0.04797	2.71	1.55	0.058
	σ		N_5–C_6	σ*	0.05187	2.77	1.67	0.061
	σ		C_6–N_9	σ*	0.04310	4.08	1.55	0.071
	σ		N_7–H_{11}	σ*	0.01046	1.30	1.55	0.040
N_1–C_6	σ	1.97848	N_1–C_2	σ*	0.03272	1.93	1.69	0.051
	σ		C_2–N_3	σ*	0.02963	2.73	1.71	0.061
	σ		C_2–N_7	σ*	0.04797	4.32	1.55	0.074
	σ		N_5–C_6	σ*	0.05187	2.64	1.68	0.060
	σ		C_6–N_9	σ*	0.04310	2.55	1.56	0.057
	σ		N_9–H_{14}	σ*	0.01069	0.53	1.55	0.026
	π	1.79357	N_1–C_6	π*	0.24849	0.53	0.55	0.015
	π		C_2–N_3	π*	0.30940	52.38	0.56	0.157
	π		C_4–N_5	π*	0.23217	17.39	0.70	0.990
	π		N_9–H_{14}	σ*	0.01069	1.66	0.99	0.038
	π		N_9–H_{15}	σ*	0.01042	1.40	0.99	0.035
C_2–N_3	σ	1.98007	N_1–C_2	σ*	0.03272	2.56	1.67	0.058
	σ		N_1–C_6	σ*	0.03917	0.53	1.66	0.027
	σ		C_2–N_7	σ*	0.04797	2.46	1.53	0.055
	σ		N_3–C_4	σ*	0.06695	2.00	1.68	0.052
	σ		C_4–N_5	σ*	0.01719	2.20	2.27	0.063

Table 7 (*continued*)

Donor (i)	Type	ED/e (a.u)[a]	Acceptor (j)	Type	ED/e (a.u)[a]	$E^{(2)}$ (kJ mol^{-1})[b]	$E(j)-E(i)$ (a.u)[c]	$F(i,j)$ (a.u)[d]
	σ		C_4–N_8	σ*	0.08617	4.07	1.56	0.072
	σ		N_7–H_{10}	σ*	0.01086	1.38	1.52	0.041
	π	1.77091	N_1–C_6	π*	0.24849	25.24	0.53	0.104
	π		C_2–N_3	π*	0.30940	1.80	0.53	0.028
	π		C_4–N_5	π*	0.23217	48.65	0.67	0.162
C_2–N_7	σ	1.98451	N_1–C_2	σ*	0.03272	1.73	1.61	0.047
	σ		N_1–C_6	σ*	0.03917	1.75	1.61	0.048
	σ		C_2–N_3	σ*	0.02963	1.49	1.63	0.044
	σ		N_3–C_4	σ*	0.06695	1.67	1.63	0.047
	σ		N_7–H_{10}	σ*	0.01086	3.18	1.47	0.061
	σ		N_7–H_{11}	σ*	0.01046	3.15	1.47	0.061
N_3–C_4	σ	1.97953	N_1–C_2	σ*	0.03272	2.82	1.68	0.062
	σ		C_2–N_3	σ*	0.02963	2.42	1.70	0.057
	σ		C_2–N_7	σ*	0.04797	4.32	1.54	0.073
	σ		C_4–N_8	σ*	0.08617	2.22	1.57	0.054
	σ		N_5–C_6	σ*	0.05187	1.18	1.66	0.040
	σ		N_8–H_{12}	σ*	0.01090	0.53	1.58	0.026
C_4–N_5	σ	1.99570	N_1–C_6	σ*	0.03917	0.79	2.14	0.037
	σ		C_6–N_9	σ*	0.04310	1.52	2.01	0.050
	π	1.86085	N_1–C_6	π*	0.24849	32.50	0.69	0.138
	π		C_2–N_3	π*	0.30940	12.25	0.70	0.086
	π		N_8–H_{12}	σ*	0.01090	1.06	1.17	0.032
	π		N_8–H_{13}	σ*	0.01100	1.35	1.17	0.037
C_4–N_8	σ	1.97901	**C_2–N_3**	σ*	0.02963	2.16	1.59	0.052
	σ		**N_3–C_4**	σ*	0.06695	1.48	1.58	0.044
	σ		**N_5–C_6**	σ*	0.05187	8.64	1.55	0.104
	σ		**N_8–H_{12}**	σ*	0.01090	3.38	1.46	0.063
	σ		**N_8–H_{13}**	σ*	0.01100	2.84	1.47	0.058
N_5–C_6	σ	1.96850	N_1–C_6	σ*	0.03917	3.43	1.69	0.068
	σ		N_3–C_4	σ*	0.06695	5.50	1.71	0.087
	σ		C_4–N_8	σ*	0.08617	11.38	1.59	0.122
	σ		C_6–N_9	σ*	0.04310	2.01	1.56	0.050
	σ		N_9–H_{15}	σ*	0.01042	0.51	1.56	0.025
C_6–N_9	σ	1.98471	N_1–C_2	σ*	0.03272	1.88	1.60	0.049
	σ		N_1–C_6	σ*	0.03917	1.70	1.60	0.047
	σ		C_4–N_5	σ*	0.01719	1.07	2.20	0.043
	σ		N_5–C_6	σ*	0.05187	2.20	1.59	0.053
	σ		N_9–H_{14}	σ*	0.01069	3.16	1.47	0.061
	σ		N_9–H_{15}	σ*	0.01042	3.18	1.47	0.061
N_7–H_{10}	σ	1.98866	N_1–C_2	σ*	0.03272	1.31	1.55	0.040
	σ		C_2–N_3	σ*	0.02963	2.01	1.57	0.050
	σ		C_2–N_7	σ*	0.04797	4.33	1.41	0.070
	σ		N_7–H_{11}	σ*	0.01046	3.44	1.41	0.062
N_7–H_{11}	σ	1.98848	N_1–C_2	σ*	0.03272	2.14	1.55	0.052
	σ		C_2–N_3	σ*	0.02963	1.27	1.57	0.040
	σ		C_2–N_7	σ*	0.04797	4.16	1.41	0.069
	σ		N_7–H_{10}	σ*	0.01086	3.48	1.41	0.062
N_8–H_{12}	σ	1.98583	N_3–C_4	σ*	0.06695	0.55	1.52	0.026
	σ		C_4–N_5	π*	0.23217	2.68	1.08	0.051
	σ		C_4–N_8	σ*	0.08617	4.23	1.40	0.070
	σ		N_8–H_{13}	σ*	0.01100	3.48	1.41	0.063
N_8–H_{13}	σ	1.98684	C_4–N_5	π*	0.23217	2.67	1.07	0.051
	σ		C_4–N_8	σ*	0.08617	4.41	1.40	0.071
	σ		N_8–H_{12}	σ*	0.01090	3.49	1.40	0.063
N_9–H_{14}	σ	1.98423	N_1–C_6	σ*	0.03917	0.64	1.54	0.028
	σ		N_1–C_6	π*	0.24849	3.24	0.97	0.053
	σ		C_6–N_9	σ*	0.04310	4.13	1.41	0.069
	σ		N_9–H_{15}	σ*	0.01042	3.39	1.41	0.062
N_9–H_{15}	σ	1.98430	N_1–C_6	π*	0.24849	3.24	0.97	0.053
	σ		N_5–C_6	σ*	0.05187	0.61	1.53	0.027
	σ		C_6–N_9	σ*	0.04310	4.09	1.41	0.068
	σ		N_9–H_{14}	σ*	0.01069	3.39	1.41	0.062
C_2	CR (1)	1.99988	C_2–N_7	σ*	0.04797	0.70	11.76	0.082
C_4	CR (1)	1.99818	N_3–C_4	σ*	0.06695	2.29	11.84	0.150
C_4	CR (1)		C_4–N_5	σ*	0.01719	7.32	12.43	0.270
C_4	CR (1)		C_4–N_8	σ*	0.08617	3.75	11.72	0.191
N_5	CR (1)	1.99929	N_3–C_4	σ*	0.06695	0.80	15.95	0.103
N_5	CR (1)		C_4–N_5	σ*	0.01719	2.57	16.54	0.185
N_5	CR (1)		N_5–C_6	σ*	0.05187	3.13	15.92	0.202

(*continued on next page*)

Table 7 (*continued*)

Donor (i)	Type	ED/e (a.u)[a]	Acceptor (j)	Type	ED/e (a.u)[a]	$E^{(2)}$ (kJ mol^{-1})[b]	$E(j)-E(i)$ (a.u)[c]	$F(i,j)$ (a.u)[d]
C_6	CR (1)	1.99987	C_6–N_9	σ^*	0.04310	0.60	11.78	0.076
N_1	LP (1)	1.95662	C_2–N_3	σ^*	0.02963	6.47	1.34	0.083
N_1	LP (1)		C_2–N_7	σ^*	0.04797	5.48	1.18	0.072
N_1	LP (1)		N_5–C_6	σ^*	0.05187	7.52	1.31	0.089
N_1	LP (1)		C_6–N_9	σ^*	0.04310	5.57	1.19	0.073
N_3	LP (1)	1.95983	N_1–C_2	σ^*	0.03272	7.38	1.29	0.087
N_3	LP (1)		C_2–N_7	σ^*	0.04797	5.81	1.15	0.073
N_3	LP (1)		C_4–N_5	σ^*	0.01719	6.70	1.89	0.101
N_3	LP (1)		C_4–N_8	σ^*	0.08617	5.76	1.19	0.075
N_5	LP (1)	1.88685	N_1–C_6	σ^*	0.03917	9.41	1.23	0.098
N_5	LP (1)		N_3–C_4	σ^*	0.06695	32.21	1.25	0.181
N_5	LP (1)		C_4–N_8	σ^*	0.08617	26.76	1.13	0.156
N_5	LP (1)		C_6–N_9	σ^*	0.04310	8.33	1.10	0.087
N_7	LP (1)	1.87268	C_2–N_3	π^*	0.30940	52.58	0.53	0.156
N_8	LP (1)	1.95343	N_3–C_4	σ^*	0.06695	8.04	1.08	0.084
N_8	LP (1)		C_4–N_5	σ^*	0.01719	6.10	1.66	0.091
N_8	LP (1)		C_4–N_5	π^*	0.23217	11.28	0.63	0.079
N_8	LP (1)		N_5–C_6	σ^*	0.05187	0.59	1.05	0.022
N_9	LP (1)	1.93154	N_1–C_6	σ^*	0.03917	9.02	1.09	0.089
N_9	LP (1)		N_1–C_6	π^*	0.24849	14.87	0.52	0.083
N_9	LP (1)		N_5–C_6	σ^*	0.05187	9.97	1.08	0.093
N_1–C_6	π^*	0.24849	C_4–N_5	π^*	0.23217	27.89	0.14	0.116
	π^*		N_9–H_{14}	σ^*	0.01069	0.78	0.44	0.046
	π^*		N_9–H_{15}	σ^*	0.01042	0.88	0.44	0.049
C_2–N_3	π^*	0.30940	C_4–N_5	π^*	0.23217	31.79	0.14	0.114
C_4–N_5	π^*	0.23217	N_8–H_{12}	σ^*	0.01090	1.18	0.33	0.051
	π^*		N_8–H_{13}	σ^*	0.01100	0.87	0.33	0.044

[a] ED/e is the electron density of donor and acceptor of NBO orbitals.
[b] $E^{(2)}$ means energy of hyper conjugative interaction (stabilization energy).
[c] $E(j)-E(i)$ is the energy difference between donor and acceptor i and j NBO orbitals.
[d] $F(I,j)$ is the Fock matrix element between i and j NBO orbitals.

$$E^{(2)} = \Delta E_{ij} = q_i F(i,j)^2/\varepsilon_j - \varepsilon_i$$

Natural bond orbital analysis provides an efficient method for studying intra and intermolecular bonding and interaction among bonds, and also provides a convenient basis for investigating charge transfer or conjugative interaction in molecular systems [29]. Some electron donor orbital, acceptor orbital and the interacting stabilization energy resulted from the second-order micro-disturbance theory [30] are where q_i is the donor orbital occupancy, are ε_i and ε_j diagonal elements and $F(i,j)$ is the off diagonal NBO Fock matrix element reported [31,32]. The larger the $E^{(2)}$ value, the more intensive is the interaction between electron donors and electron acceptors, i.e. the more donating tendency from electron donors to electron acceptors and the greater the extent of conjugation of the whole system [33]. Delocalization of electron density between occupied Lewis-type (bond or lone pair) NBO orbitals and formally unoccupied (anti-bond or Rydgberg) non-Lewis NBO orbitals correspond to a stabilizing donor–acceptor interaction. NBO analysis has been performed on the melamine molecule at the DFT/B3LYP/6-311++G(d,p) level in order to elucidate the delocalization of electron density within the molecule.

The strong intra molecular hyper conjucation interaction of the σ and π electrons of N–C to the C–N bond in the ring leads to stabilization of some part of the ring as evident from Table 7. The intramolecular interactions are formed by the orbital overlapping between N–C, C–N anti-bond orbital which results intramolecular charge transfer (ICT) causing stabilizations are observed as increase in electron density (ED) in N–C, C–N anti-bonding orbital that weakens the respective bonds. The intra molecular hyper conjugative interactions of $\pi(N_1$–$C_6)$ to $\pi^*(C_2$–$N_3)$ leads to highest stabilization of 52.38 kJ mol^{-1}. In case of $\pi(C_2$–$N_3)$ orbital the $\pi^*(N_1$–$C_6)$, $\pi^*(C_4$–$N_5)$ shows the stabilization energy of 25.24 kJ mol^{-1} and 48.65 kJ mol^{-1}. Similarly in the case of $\pi(C_4$–$N_5)$ to $\pi^*(N_1$–$C_6)$ leads to stabilization energy of 32.50 kJ mol^{-1} and LP(1)N_7 to $\pi^*(C_2$–$N_3)$ shows the highest stabilization of 52.58 kJ mol^{-1}.

Table 8
Theoritically computed zero-point vibrational energy (K cal mol^{-1}), rotational constants (GHZ), rotational temperature (kelvin), thermal energy (K cal mol^{-1}), molar capacity at constant volume (cal mol^{-1} kelvin^{-1}), entropy (cal mol^{-1} kelvin^{-1}) and dipole moment (debyes).

Parameter	B3LYP	
	6-31G(d,p)	6-311++G(d,p)
Zero-point vibrational energy	73.163	77.827
Rotational constant	2.013	2.061
	2.013	2.061
	1.007	1.031
Rotational temperature	0.097	0.099
	0.097	0.099
	0.048	0.049
Energy		
Total	78.320	83.015
Translational	0.889	0.889
Rotational	0.889	0.889
Vibrational	76.542	81.238
Molecular capacity at constant volume		
Total	31.817	30.451
Translational	2.981	2.981
Rotational	2.981	2.981
Vibrational	25.855	24.489
Entropy		
Total	86.975	87.931
Translational	40.409	40.409
Rotational	28.756	28.687
Vibrational	17.811	18.836
Dipole moment		
μ_x	0.006	−0.033
μ_y	0.025	0.027
μ_z	0.581	0.298
μ_{total}	0.581	0.301

Other molecular properties

Several calculated thermodynamical parameters such as the zero-point vibrational energies (ZPVE), the energy, $S_{vib}(T)$, the molecular capacity at constant volume, rotational constants and rotational temperature have been presented in Table 8. The various thermodynamical parameters in the ZPVEs seem to be significant. The total energies are found to decrease with the increase of the basis set dimension. The rotational constant and rotational temperature values are somewhat higher when calculated by B3LYP/6-31G(d,p) than B3LYP/6-311++G(d,p). From Table 8, it is clear that as the rotational temperature increases, there will be a change of rational constant value. The changes in the total entropy of melamine at room temperature at different basis set are only marginal.

Conclusion

The present investigation thoroughly analyzed the vibrational spectra, both FT-IR and FT-Raman of melamine. All the vibrational bands observed in the FT-IR and FT-Raman spectra of melamine are assigned to the various modes of vibrations. The complete vibrational assignments of wavenumbers are made on the basis of the Total energy distribution (TED). The optimized geometrical parameters calculated at B3LYP/6-31G(d,p) basis set are slightly larger than those calculated at B3LYP/6-311++G(d,p). HOMO and LUMO energy gaps explain the eventual charge transfer interactions taking place within the molecule. NBO result reflects the charge transfer within the molecule.

References

[1] B. Gibson Weldon, SRI: The Founding Years, Stanford Research Institute, 1980. ISBN 0-913232-80-7.
[2] Anne Field (2003-06-24). "Melamine Plastic". Home Maintenance and Repair. Michigan State University Extension.
[3] "The Rise and Fall of Melamine Tableware". plastiquarian (Plastics Historical Society) (32): 10. Summer 2004. Archived from the original on 2008-06-25. Retrieved 2008-12-12.
[4] World Health Organization: Melamine and Cyanuric Acid: Toxity. Preliminary Risk Assessment and Guidance on Levels in Food. World Health Organization: September 25, 2008.
[5] E. Nicoleta, Mircescu, M. Oltean, V. Chis, N. Leopold, Vib. Spect. 62 (2012) 165–171.
[6] Gaung Pu, Xue Yu, Gung Pu, Pen Xi, PubMed 32 (2012) 703–707.
[7] M.J. Frisch, G.W. Trucks, H.B. Schlegel, G.E. Scuseria, M.A. Robb, J.R. Cheeseman, J.A. Montgomery, Jr., T. Vreven, K.N. Kudin, J.C. Burant, J.M. Millam, S.S. Iyengar, J. Tomasi, V. Barone, B. Mennucci, M. Cossi, G. Scalmani, N. Rega, G.A. Petersson, H. Nakatsuji, M. Hada, M. Ehara, K. Toyota, R. Fukuda, J. Hasegawa, M. Ishida, T. Nakajima, Y. Honda, O. Kitao, H. Nakai, M. Klene, X. Li, J.E. Knox, H.P. ratchian, J.B. Cross, C. Adamo, J. Jaramillo, R. Gomperts, R.E. Stratmann, O. Yazyev, A.J. Austin, R. Cammi, C. Pomelli, J.W. Ochterski, P.Y. Ayala, K. Morokuma, G.A. Voth, P. Salvador, J.J. Dannenberg, V.G. Zakrzewski, S. Dapprich, A.D. Daniels, M.C. Strain, O. Farkas, D.K. Malick, A.D. Rabuck, K. Raghavachari, J.B. Foresman, J.V. Ortiz, Q. Cui, A.G. Baboul, S. Clifford, J. Cioslowski, B.B. Stefanov, G. Liu, A. Liashenko, P. Piskorz, I. Komaromi, R.L. Martin, D.J. Fox, T. Keith, M.A. Al-Laham, C.Y. Peng, A. Nanayakkara, M. Challacombe, P.M.W. Gill, B. Johnson, W. Chen, M.W. Wong, C. Gonzalez, J.A. Pople, Gaussian 03, Revision A.1, Gaussian Inc, Pittsburgh, PA, 2003.
[8] A. Grigority Zhurko, A. Denis Zhurko, Chemcraft program, Academic version 1.5, 2004.
[9] J.K. Wilmshust, H.J. Bernstein, Can. J. Chem. 35 (1957) 911–919.
[10] D. Sajan, J. Binoy, B. Pradeep, K. Venkatakrishnan, V.B. Kartha, I.H. Joe, V.S. Jayakumar, Spectrochim. Acta A60 (2004) 173–180.
[11] E.D. Glendening, A.E. Reed, J.E. Carpenten, F. Weinhold, NBO Version 3.1, TCI, University of Wisconsin, Madison, 1998.
[12] A. Cousson, B. Nicola, F. Fillaux, Acta Crystallogr. E 61 (2005) 222–224.
[13] M. Silverstein, G. Clayton Basseler, C. Morill, Spectrometric Identification of Organic Compounds, Wiley, New York, 1981.
[14] R. Shanmugam, D. Sathyanarayana, Spectrochim. Acta 40A (1984) 764–770.
[15] N. Sundaraganesan, S. Ayyappan, H. Umamaheswari, B. Domnic Joshua, Spectrochim. Acta 66A (2007) 17–27.
[16] P. Mani, H. Umamaheswari, B. Dominic Joshua, N. Sundaraganesan, J. Mol. Struct. (Theochem.) 863 (2008) 44–49.
[17] M. Arivazhagan, V. Krishnakumar, R. John Xavier, G. Ilango, V. Balachandran, Spectrochim. Acta Part A 72 (2009) 941–946.
[18] V. Krishnakumar, R. John Xavier, Spectrochim. Acta Part A 60 (2004) 709–714.
[19] C.H. Choi, M. Kertez, J. Phys. Chem. 101A (1997) 3823–3831.
[20] S. Gunasekaran, R. Arun Balaji, S. Kumaresan, G. Anand, S. Srinivasan, Can. J. Anal. Sci. Spectrosc. 53 (2008) 149–162.
[21] L. Padmaja, C. Ravikumar, D. Sajan, I.H. Joe, V.S. Jayakumar, G.R. Pettit, O.F. Nielson, J. Raman Spectrosc. 40 (2009) 419–428.
[22] C. Ravikumar, I.H. Joe, V.S. Jayakumar, Chem. Phys. Lett. 460 (2008) 552–558.
[23] A. Pirnau, V. Chis, O. Oniga, N. Leopold, L. Szabo, M. Baias, O. Cozar, Vib. Spectrosc. 48 (2008) 289–296.
[24] V.M. Geskin, C. Lambert, J.L. Bredas, J. Am. Chem. Soc. 125 (2003) 15651–15658.
[25] D. Sajan, I.H. Joe, V.S. Jayakumar, J. Zaleski, J. Mol. Struct. 785 (2006) 43–53.
[26] D.A. Kleinman, Phys. Rev. 126 (1962) 1977–1979.
[27] J.S. Murray, K. Sen, Molecular Electrostatic Potential Concepts and Applications, Elsevier Science B.V, Amsterdam, The Netherlands, 1996.
[28] M. Alcolea Palafox, Int. J. Quent. Chem. 77 (2000) 661–684.
[29] S. Subhashandrabose, R. Akhil, R. Krishnan, H. Saleem, R. Parameswari, N. Sundaraganesan, V. Thanikachalam, G. Manikandan, Spectrochim. Acta 77A (2010) 877–884.
[30] J.N. Liu, Z.R. Chen, S.F. Yuan, J. Zhejiang, Uni. Sci. B 6 (2005) 584–589.
[31] C. James, A. Amalraj, A. Regunathan, V.S. Jayakumar, I.H. Joe, J. Raman Spectrosc. 37 (2006) 1381–1392.
[32] A.R. Krishanan, H. Saleem, S. Subhashandrabose, N. Sundaraganesan, S. Sebastian, Spetrochim. Acta A78 (2011) 582–589.
[33] S. Sebastian, N. Sundaraganesan, Specrochim. Acta 75A (2010) 941–952.